

BIORTHOGONAL SPLINES FOR OPTIMAL WEAK PATCH-COUPLING IN ISOGEOMETRIC ANALYSIS WITH APPLICATIONS TO FINITE DEFORMATION ELASTICITY

LINUS WUNDERLICH, ALEXANDER SEITZ, MERT DENIZ ALAYDIN,
BARBARA WOHLMUTH, AND ALEXANDER POPP

ABSTRACT. A new construction of biorthogonal splines for isogeometric mortar methods is proposed. The biorthogonal basis has a local support and, at the same time, optimal approximation properties, which yield optimal results with mortar methods. We first present the univariate construction, which has an inherent crosspoint modification. The multivariate construction is then based on a tensor product for weighted integrals, whereby the important properties are inherited from the univariate case. Numerical results including large deformations confirm the optimality of the newly constructed biorthogonal basis.

1. INTRODUCTION

Weak patch-coupling is an important feature for practical applications of isogeometric analysis (IGA). With isogeometric methods, the computational domain is usually divided into several spline patches [1, 2, 3, 4] and the solution to a partial differential equation is approximated by spline functions [5] on each patch. Typically, multivariate splines are defined based on a tensor-product structure and a flexible coupling between the patches is important to gain some flexibility of the local meshes. Different approaches are considered, e.g., Nitsche's method [6, 7], penalty based methods [8] and mortar methods [9, 10], and there is a recent interest in higher-order couplings, see, e.g. [11, 12]. A recent practical review, which includes the related issue of trimming, is given in [13]. Besides patch-coupling, these methods are also used for the discretization of contact problems, see, e.g., [14, 15] and the references therein.

Mortar methods were originally applied in spectral and finite element methods [16, 17, 18], and for the isogeometric case a mathematical stability and a priori analysis can be found in [19]. The use of dual mortar methods [20] yields computational advantages also for contact discretizations [21, 22, 23, 24]. However, already

(B. Wohlmuth, L. Wunderlich) M2 - ZENTRUM MATHEMATIK, TECHNISCHE UNIVERSITÄT MÜNCHEN, BOLTZMANNSTRASSE 3, 85748 GARCHING, GERMANY

(A. Seitz) INSTITUTE FOR COMPUTATIONAL MECHANICS, TECHNISCHE UNIVERSITÄT MÜNCHEN, BOLTZMANNSTRASSE 15, 85748 GARCHING, GERMANY

(M.D. Alaydin) SCHOOL OF ENGINEERING, BROWN UNIVERSITY, 182 HOPE STREET, PROVIDENCE, RI 02912, USA

(A. Popp) INSTITUTE FOR MATHEMATICS AND COMPUTER-BASED SIMULATION, UNIVERSITÄT DER BUNDESWEHR MÜNCHEN, WERNER-HEISENBERG-WEG 39, 85577 NEUBIBERG, GERMANY

E-mail addresses: (L. Wunderlich) `linus.wunderlich@ma.tum.de`, (A. Seitz) `seitz@lmm.mw.tum.de`, (M.D. Alaydin) `mert.alaydin@brown.edu`, (B. Wohlmuth) `wohlmuth@ma.tum.de`, (A. Popp, Corresponding author) `alexander.popp@unibw.de`.

Funds provided by the Deutsche Forschungsgemeinschaft under the contract/grant numbers: WO 671/11-1 as well as PO1883/1-1, WA1521/15-1 and WO 671/15-1 (within the Priority Programme SPP 1748, "Reliable Simulation Techniques in Solid Mechanics. Development of Non-standard Discretisation Methods, Mechanical and Mathematical Analysis") are gratefully acknowledged.

for finite element methods the use of dual mortar methods for higher order methods poses additional difficulties, which could be solved by a local change of the primal basis [25, 26, 27]. The straightforward use of dual isogeometric mortar methods was considered in [28], where a well-behavior for contact problems was observed, while for patch-coupling the convergence rate was severely reduced. Here, we present a new construction of local dual basis functions with optimal approximation properties, based on the construction given in [29] for the finite element context. For the first time, this scheme allows to combine the two crucial features of local support of the dual basis and optimal approximation properties. Alternative approaches include the use of basis functions that are not dual, but have a more convenient sparsity structure than standard basis functions [30]. Very recently, it has been proposed in [31] to refine one layer of elements along the interfaces to obtain a matching mesh. In the case of non-matching parametrizations, the mesh does not necessarily match even though the knots do match, so an unknown number of extra refinements is necessary. Also, the extension to a general three-dimensional setting remains unclear.

This article is structured as follows. In the next section, we state the problem setting and briefly present standard isogeometric methods. In Section 3 we present the construction of the local dual basis functions with optimal approximation properties for one-dimensional and two-dimensional interfaces. The newly constructed dual basis functions are applied to isogeometric patch-coupling in Section 4 and the results of this work are summarized in Section 5.

2. PROBLEM SETTING AND RECAP OF ISOGEOMETRIC MORTAR METHODS

Let $\Omega \subset \mathbb{R}^d$, $d = 2, 3$ be a bounded domain with a piecewise smooth boundary, which is decomposed into two open sets Γ_D, Γ_N , such that $\Gamma_D \cap \Gamma_N = \emptyset$ and $\bar{\Gamma}_D \cup \bar{\Gamma}_N = \partial\Omega$. The reference domain Ω with its points \mathbf{X} is mapped at any instance of time t to the deformed configuration $\Omega^{(t)}$ with its points \mathbf{x} via the orientation preserving, invertible mapping $\phi_t : \Omega \rightarrow \Omega^{(t)}$, $\mathbf{X} \mapsto \mathbf{x}(\mathbf{X})$, which defines the displacement field $\mathbf{u} = \mathbf{x}(\mathbf{X}) - \mathbf{X}$. Starting from the deformation gradient $\mathbf{F} = \text{Id} + \frac{\partial \mathbf{u}}{\partial \mathbf{X}}$, the right Cauchy–Green tensor $\mathbf{C} = \mathbf{F}^\top \mathbf{F}$ defines a non-linear measure of stretches. For simplicity, a hyperelastic material behavior is assumed, although the later presented mortar method directly applies to other constitutive relations as well. For hyperelastic materials, the existence of a strain energy function Ψ is postulated, and the second Piola–Kirchhoff stress is then defined via $\mathbf{S} = 2 \frac{\partial \Psi}{\partial \mathbf{C}}$. For homogeneous Dirichlet values, we solve the quasi-static equilibrium equations of nonlinear elasticity on the domain Ω :

$$\begin{aligned} \text{Div}(\mathbf{F}\mathbf{S}) + \hat{\mathbf{b}}_0 &= \mathbf{0} \quad \text{in } \Omega, \\ \mathbf{u} &= \mathbf{0} \quad \text{on } \Gamma_D, \\ (\mathbf{F}\mathbf{S})\mathbf{N} &= \hat{\mathbf{t}}_0 \quad \text{on } \Gamma_N, \end{aligned}$$

where \mathbf{N} denotes the outward unit-normal on Γ_N , $\hat{\mathbf{b}}_0$ a body force vector per unit undeformed volume and $\hat{\mathbf{t}}_0$ a given first Piola–Kirchhoff traction vector.

In the following, we briefly present the isogeometric mortar methods. For a more detailed presentation and the use of trace space Lagrange multipliers, see [19], for the extension to contact problems, see [28].

2.1. Standard spline spaces. Let a spline degree p and an open knot vector (i.e., first and last $p + 1$ entries are repeated) $\Xi = (\xi_1, \dots, \xi_{n+p+1})$ be given. The entries of Ξ without their repetitions form the break point vector $Z = (\zeta_1, \dots, \zeta_E)$, and m_i denotes the multiplicity of ζ_i in Ξ . The Cox-de Boor recursion formula then defines the spline basis functions \hat{B}_i^p , $i = 1, \dots, n$ and the corresponding spline space

$\widehat{S}^p(\Xi) = \text{span}_i \widehat{B}_i^p$ in the univariate setting. In the multivariate setting, consider $\Xi = \Xi_1 \times \cdots \times \Xi_d$ and the B-spline basis $\widehat{B}_i^p(\zeta) = \widehat{B}_{i_1}^p(\zeta_1) \cdots \widehat{B}_{i_d}^p(\zeta_d)$ with the spline space $\widehat{S}^p(\Xi) = \bigotimes_{\delta=1}^d \widehat{S}^p(\Xi_\delta) = \text{span}_i \widehat{B}_i^p$. For simplicity of notation, we consider the same polynomial degree in all directions.

Introducing positive weights $w_i > 0$ and the corresponding weight function $\widehat{W}(\zeta) = \sum_{i \in \mathbb{I}} w_i B_i^p(\zeta)$, we define the NURBS basis and space as

$$\widehat{N}_i^p(\zeta) = \widehat{B}_i^p(\zeta) / \widehat{W}(\zeta), \quad \widehat{N}^p(\Xi) = \{\widehat{v}_h = \widehat{w}_h / \widehat{W}, \quad \widehat{w}_h \in \widehat{S}^p(\Xi)\}.$$

2.2. Description of the computational domain. We consider a decomposition of the domain Ω into K non-overlapping domains Ω_k :

$$\overline{\Omega} = \bigcup_{k=1}^K \overline{\Omega}_k, \quad \text{and } \Omega_i \cap \Omega_j = \emptyset \text{ for } i \neq j.$$

For $1 \leq k_1, k_2 \leq K$, $k_1 \neq k_2$, the interface is defined as the interior of the intersection of the boundaries, i.e., $\overline{\Gamma}_{k_1 k_2} = \partial\Omega_{k_1} \cap \partial\Omega_{k_2}$, where $\Gamma_{k_1 k_2}$ is open. The non-empty interfaces are enumerated as Γ_l , $l = 1, \dots, L$. For each interface, one of the adjacent subdomains is chosen as the master side $m(l)$, the other one as the slave side $s(l)$, i.e., $\overline{\Gamma}_l = \partial\Omega_{m(l)} \cap \partial\Omega_{s(l)}$. The slave side is used to define the Lagrange multiplier space that enforces the coupling between the master and the slave side.

Each subdomain Ω_k is given as the image of the parametric space $\widehat{\Omega} = (0, 1)^d$ by one single NURBS parametrization $\mathbf{F}_k: \widehat{\Omega} \rightarrow \Omega_k$, $\mathbf{F}_k \in (N^p(\Xi))^d$, which satisfies the regularity Assumption [19, Assumption 1]: The parametrization \mathbf{F}_k is a bi-Lipschitz homeomorphism, $\mathbf{F}_k|_{\overline{\mathbf{Q}}} \in C^\infty(\overline{\mathbf{Q}})$ and $\mathbf{F}_k^{-1}|_{\overline{\mathbf{O}}} \in C^\infty(\overline{\mathbf{O}})$ for any elements $\overline{\mathbf{Q}}$ and $\overline{\mathbf{O}}$ of the parametric and the physical mesh, respectively.

Furthermore, we assume that the decomposition represents the Dirichlet boundary in the sense, that the pull-back of $\partial\Omega_k \cap \Gamma_D$ is either empty or the union of whole faces of the unit d -cube. We furthermore assume to be in a slave conforming situation, i.e., for each interface, the pull-back with respect to the slave domain is a whole face of the unit d -cube in the parametric space. The h -refinement procedure yields a family of meshes, with each mesh being a uniform refinement of the initial one.

2.3. The variational forms. For each subdomain Ω_k , we consider the local space $H_D^1(\Omega_k) = \{v_h \in H^1(\Omega_k) : v_h|_{\partial\Omega_k \cap \Gamma_D} = 0\}$ and define the global broken Sobolev spaces $V = \prod_{k=1}^K H_D^1(\Omega_k)$ and $M = \prod_{l=1}^L H^{-1/2}(\Gamma_l)$, endowed with the broken norms $\|v\|_V^2 = \sum_{k=1}^K \|v\|_{H^1(\Omega_k)}^2$ and $\|v\|_M^2 = \sum_{l=1}^L \|v\|_{H^{-1/2}(\Gamma_l)}^2$.

Defining $\mathbf{V} = (V)^d$ and $\mathbf{M} = (M)^d$, we consider the broken non-linear form $a: \mathbf{V} \times \mathbf{V} \rightarrow \mathbb{R}$ and the linear form $f_{\text{ext}}: \mathbf{V} \rightarrow \mathbb{R}$:

$$a(\mathbf{u}, \mathbf{v}) = \sum_{k=1}^K \int_{\Omega_k} (\mathbf{F}\mathbf{S}) : \text{Grad } \mathbf{v} \, d\mathbf{X}, \quad f_{\text{ext}}(\mathbf{v}) = \sum_{k=1}^K \int_{\partial\Omega_k \cap \Gamma_N} \hat{\mathbf{t}}_0^\top \mathbf{v} \, d\Gamma + \int_{\Omega_k} \hat{\mathbf{b}}_0^\top \mathbf{v} \, d\mathbf{X}.$$

2.4. Isogeometric mortar discretization. In the following, we define our discrete approximation spaces used in the mortar context, the mortar saddle point problem and the convergence order. We introduce $V_{k,h}$ as the approximation space on Ω_k by

$$V_{k,h} = \{v_k = \widehat{v}_k \circ \mathbf{F}_k^{-1} \in H_D^1(\Omega_k), \widehat{v}_k \in \widehat{N}^{p_k}(\Xi_k)\},$$

which is defined on the knot vector Ξ_k of degree p_k , with $\mathbf{V}_{k,h} = (V_{k,h})^d$. On Ω , we define the product space $\mathbf{V}_h = \prod_{k=1}^K \mathbf{V}_{k,h} \subset \mathbf{V}$, which forms an $(H^1(\Omega))^d$ non-conforming space as it is discontinuous over the interfaces.

The mortar method is based on a weak enforcement of continuity across the interfaces Γ_l in broken Sobolev spaces. Let a space of discrete Lagrange multipliers $M_{l,h} \subset L^2(\Gamma_l)$ on each interface Γ_l be given. On the skeleton Γ , we define the discrete product Lagrange multiplier space \mathbf{M}_h as $\mathbf{M}_h = \prod_{l=1}^L M_{l,h}^d$.

One possibility for a mortar method is to specify the discrete weak formulation as a saddle point problem: Find $(\mathbf{u}_h, \boldsymbol{\lambda}_h) \in \mathbf{V}_h \times \mathbf{M}_h$, such that

$$(1a) \quad a(\mathbf{u}_h, \mathbf{v}_h) + b(\mathbf{v}_h, \boldsymbol{\lambda}_h) = f_{\text{ext}}(\mathbf{v}_h), \quad \mathbf{v}_h \in \mathbf{V}_h,$$

$$(1b) \quad b(\mathbf{u}_h, \boldsymbol{\mu}_h) = 0, \quad \boldsymbol{\mu}_h \in \mathbf{M}_h,$$

where $b(\mathbf{v}, \boldsymbol{\mu}) = \sum_{l=1}^L \int_{\Gamma_l} \rho \boldsymbol{\mu}^\top [\mathbf{v}]_l \, d\Gamma$ includes a weight $\rho: \Gamma_l \rightarrow \mathbb{R}$ and $[\cdot]_l$ denotes the jump from the master to the slave side over Γ_l . The standard choice $\rho = 1$ will be altered in the three-dimensional case to simplify the construction of the Lagrange multiplier.

Due to the jump term, the coupling term decomposes in two integrals:

$$\int_{\Gamma_l} \rho \boldsymbol{\mu}^\top [\mathbf{v}]_l \, d\Gamma = \int_{\Gamma_l} \rho \boldsymbol{\mu}^\top \mathbf{v}_s \, d\Gamma - \int_{\Gamma_l} \rho \boldsymbol{\mu}^\top \mathbf{v}_m \, d\Gamma,$$

where the second one includes the product of functions defined on the slave domain and the master domain on the interface. As we assume the subdomains to match at the interface, the identity mapping on the geometric space suits as a projection between the spaces. In contrast, the isogeometric parametrizations of both subdomains are independent and may not match. To map a point $\boldsymbol{\zeta}_s$ in the parametric domain of the slave side to the equivalent point $\boldsymbol{\zeta}_m$ in the parametric domain of the master side, the inverse of the master geometry mapping is applied:

$$\boldsymbol{\zeta}_m = \mathbf{F}_m^{-1}(\mathbf{F}_s(\boldsymbol{\zeta}_s)).$$

We note that the accurate numerical integration of the coupling terms is important to obtain an optimal method, see [32, 33, 34, 35].

2.5. Standard and biorthogonal Lagrange multiplier spaces. It is well-known from the theory of mixed and mortar methods, that two requirements guarantee the method to be well-posed and of optimal order, see [16, 18, 36]. One is a uniform inf-sup stability of the discrete spaces and the second one an approximation requirement of the Lagrange multiplier. Given a sufficient approximation order and the inf-sup stability, then [19, Theorem 6] yields optimal order convergence rates.

Several stable trace spaces exist, but the structure of the resulting equation system (1), which is of a saddle point problem, causes a high computational effort. In comparison to a purely primal system, the saddle point system has more degrees of freedom, but also the solution of the indefinite equation system is more complicated, see the discussion in [37]. Without the use of biorthogonal basis functions, the reduction to a symmetric positive definite system in the primal variable involves the inversion of a non-diagonal mass matrix and severely disturbs the sparsity of the system.

For a clear insight, let us consider the block-structure of the saddle point problem arising within each Newton step for (1) with a two-patch coupling, written in terms of the primal u and dual λ degrees of freedom:

$$\begin{pmatrix} K & M^\top \\ M & 0 \end{pmatrix} \begin{pmatrix} \Delta u \\ \lambda \end{pmatrix} = - \begin{pmatrix} f \\ 0 \end{pmatrix},$$

where $f = f_{\text{int}} - f_{\text{ext}}$.

The saddle point problem is decomposed based on the degrees of freedom u_1^S and u_1^M belonging to the slave and the master body, respectively, except the ones on

With mortar methods, special care needs to be taken with crosspoints ($d = 2$) or wirebaskets ($d = 3$) to prevent an over-constrained global equation system:

$$\partial_{CP} = \left(\bigcup_{l \neq j} \partial\Gamma_l \cap \partial\Gamma_j \right) \cup \left(\bigcup_l \partial\Gamma_l \cap \Gamma_D \right).$$

In the vicinity of crosspoints, we consider the restriction of the discrete primal space to zero boundary values: $H_{CP}^1(\Gamma_l) = \{v \in H^1(\Gamma_l), v|_{\partial_{CP}} = 0\}$ and $W_{l,h} = \{v_h|_{\Gamma_l}, v_h \in V_{s(l),h}\} \cap H_{CP}^1(\Gamma_l)$.

We consider the coupling $b(\mathbf{v}, \boldsymbol{\mu}) = \sum_{l=1}^L \int_{\Gamma_l} \rho \boldsymbol{\mu}^\top [\mathbf{v}]_l \, d\Gamma$, for each interface Γ_l individually and hence drop the index l . Furthermore, only the slave domain is considered, so we also drop the index $s(l)$. For each interface, we transform the integral to the parametric domain: For a NURBS basis function $N_i = (\widehat{B}_i \circ \mathbf{F}^{-1}) / (\widehat{\mathcal{W}} \circ \mathbf{F}^{-1})$ and a Lagrange multiplier basis $\psi_j = \widehat{\psi}_j \circ \mathbf{F}^{-1}$, we get

$$\begin{aligned} \int_{\Gamma} \rho (N_i \mathbf{e}_k)^\top (\psi_j \mathbf{e}_{k'}) \, d\Gamma &= \delta_{kk'} \int_{\Gamma} \rho N_i \psi_j \, d\Gamma \\ (4) \qquad \qquad \qquad &= \delta_{kk'} \int_{\widehat{\Gamma}} \widehat{\rho} \widehat{B}_i^p \widehat{\psi}_j \, d\widehat{\Gamma}, \end{aligned}$$

with $\widehat{\rho} = \rho \circ \mathbf{F} \det \nabla_{\widehat{\Gamma}} \mathbf{F} / \widehat{\mathcal{W}}$. We use the Kronecker delta δ_{ij} , which equals one if $i = j$ and zero otherwise. Biorthogonality is characterized by the relation

$$\int_{\widehat{\Gamma}} \widehat{\rho} \widehat{B}_i^p \widehat{\psi}_j \, d\widehat{\Gamma} = c_i \delta_{ij}.$$

We start with the one-dimensional construction and later consider the tensor-product extension based on the use of weighted but equivalent L^2 -spaces.

3.1. Unilateral construction. The biorthogonal basis with polynomial reproduction is constructed by carefully studying the required properties. It is defined within a broken space of local polynomials of the same degree, where a family of biorthogonal basis functions with local support exists. Then several local equation systems are solved to find a basis with local support and the desired polynomial reproduction.

Without loss of generality $\Gamma = \mathbf{F}((0, 1) \times \{0\})$, i.e., $\widehat{\Gamma} = (0, 1) \times \{0\}$. We consider the weighted L^2 -product $(u, v)_{\widehat{\rho}} = \int_0^1 u v \widehat{\rho} \, d\widehat{\Gamma}$ as given by (4). The trace space of B-splines on the parametric space is then given by:

$$W_h = \left\{ \widehat{v}_h = v_h \circ \mathbf{F} \widehat{\mathcal{W}} \Big|_{\widehat{\Gamma}}, v_h \in V_h \cap H_{CP}^1(\Gamma) \right\} \subset \widehat{S}^p(\boldsymbol{\Xi}_1),$$

with the basis \widehat{B}_i^p , $i \in \mathcal{I}_{\text{bsp}} = \{i_{\min}, \dots, i_{\max}\}$, where $i_{\min} \in \{1, 2\}$ and $i_{\max} \in \{n-1, n\}$, depending on ∂_{CP} .

The biorthogonal basis is constructed within the broken polynomial space of the same degree as the spline space:

$$W_h^{-1} = \{v \in L^2(0, 1), v|_{e_i} \in \mathbb{P}_p\},$$

which is of dimension $N = \dim W_h^{-1} = (E-1)(p+1)$, where $E-1$ is the number of elements on $\widehat{\Gamma}$ and $e_i = (\zeta_i, \zeta_{i+1})$. Since $W_h \subset W_h^{-1}$, we can extend the B-spline basis to a basis of the broken space. A convenient basis with the desired support is constructed in the following.

The support of the extended basis is desired not to be larger than the support of a single B-spline function. This is ensured by decomposing the broken polynomial

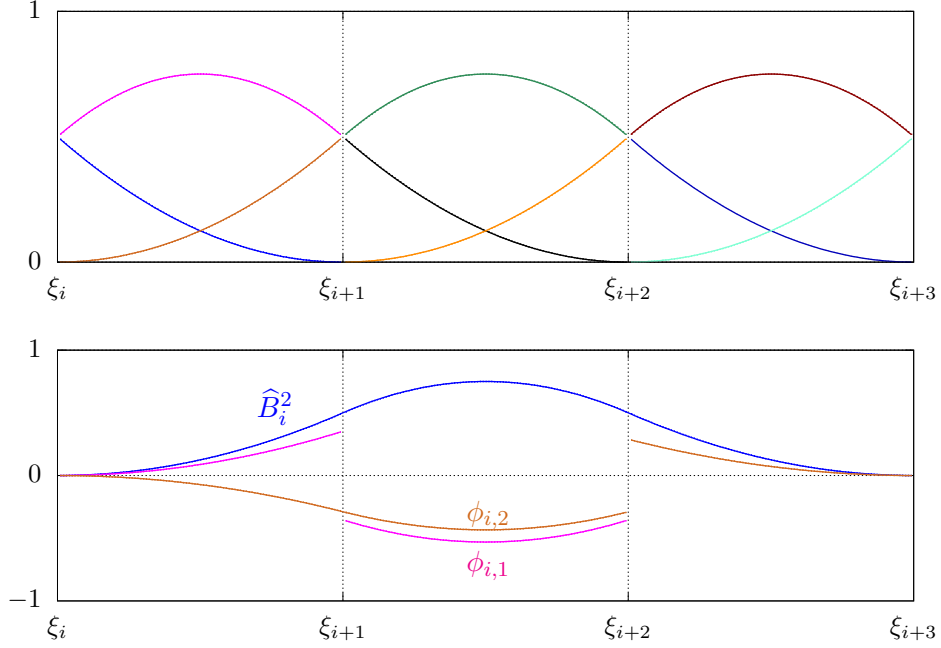


FIGURE 2. Illustration of the broken basis. Top: broken basis functions $\widehat{B}_{i,j}^2$. Bottom: Local basis $(\widehat{B}_i^2, \phi_{i,1}, \phi_{i,2})$, based on the orthogonal basis A_j (normalized).

space W_h^{-1} into n subspaces $W_{h,i}^{-1}$ by breaking apart the B-spline basis:

$$W_{h,i}^{-1} = \text{span} \left\{ \widehat{B}_i^p \Big|_{e_j}, j = 1, \dots, E-1 \right\}, \quad i = 1, \dots, n.$$

Since each basis function is supported on at most $p+1$ elements, it holds $n_i = \dim W_{h,i}^{-1} \leq p+1$, and, since B-splines form a local polynomial basis, it indeed holds that $W_h^{-1} = \bigotimes_{i=1}^n W_{h,i}^{-1}$. Within each local space $W_{h,i}^{-1}$ we extend \widehat{B}_i^p to a basis, i.e., we define $\phi_{i,j} \in W_{h,i}^{-1}$, $j = 1, \dots, n_i - 1$, such that

$$W_{h,i}^{-1} = \text{span} \left(\widehat{B}_i^p, (\phi_{i,j})_{j=1, \dots, n_i-1} \right).$$

Then, the local basis functions are combined to a basis of W_h^{-1} :

$$(\varphi_i)_{i=1, \dots, N} = (\widehat{B}_1^p, \dots, \widehat{B}_n^p, (\phi_{1,j})_{j=1, \dots, n_1-1}, \dots, (\phi_{n,j})_{j=1, \dots, n_n-1}).$$

Any choice of the local basis functions yields the desired support, but to simplify the algebraic construction of a biorthogonal basis, we consider the construction presented in the following Remark 1.

Remark 1 (Construction of the local basis functions $\phi_{i,j}$). *We describe the construction for the first $\lceil n/2 \rceil$ basis functions and note that the last basis functions can be constructed analogously, by transforming the index as $\tilde{i} = n+1-i$.*

Consider \widehat{k} , such that $\text{supp } \widehat{B}_i^p = [\zeta_{\widehat{k}}, \zeta_{\widehat{k}+n_i}]$. Then restricting \widehat{B}_i^p to each element of the support yields

$$\widehat{B}_{i,j}^p = \widehat{B}_i^p \Big|_{e_{\widehat{k}+j-1}}, \quad j = 1, \dots, n_i,$$

Based on this basis, a family of biorthogonal basis functions to the B-splines can be constructed:

$$\tilde{\psi}_i + \sum_{k \in \mathcal{J}_{\text{extra}}} z_{ki} \tilde{\psi}_k$$

for any z_{ki} , $k \in \mathcal{J}_{\text{extra}}$, $i \in \mathcal{I}_{\text{bsp}}$. Since the $\tilde{\psi}_k$ have a local support, a suitable sparse choice of the z_{ki} yields a local basis. The choice of the non-zero values is determined by local equation systems, which finish the construction.

For each $\hat{k} \in \mathcal{J}_{\text{extra}}$, let us choose an index set $\mathcal{I}_{\text{loc}}(\hat{k}) \subset \mathcal{I}_{\text{bsp}}$ with $|\mathcal{I}_{\text{loc}}(\hat{k})| = p + 1$. The choice of the index set is discussed in the following Remark 2. Let $(p_i)_{i=1, \dots, p+1}$ be a basis of \mathbb{P}_p , e.g., monomials or a set of orthogonal polynomials. Then we set $z_{\hat{k}i} = 0$ for $i \notin \mathcal{I}_{\text{loc}}(\hat{k})$ and solve the following square linear equation system for the remaining entries $z_{\hat{k}i}$, $i \in \mathcal{I}_{\text{loc}}(\hat{k})$:

$$(6) \quad \sum_{i \in \mathcal{I}_{\text{loc}}(\hat{k})} \left(p_l, \hat{B}_i^p \right)_{\hat{\rho}} z_{\hat{k}i} = (p_l, \varphi_{\hat{k}})_{\hat{\rho}}, \quad l = 1, \dots, p + 1.$$

The following diagram sketches how the sparsity structure of z_{ki} depends on $\mathcal{I}_{\text{loc}}(\hat{k})$ for $p = 2$:

$$(z_{k,i})_{k,i} : \quad \begin{array}{c} k \in \mathcal{J}_{\text{extra}} \\ \downarrow \\ \text{---} \hat{k} \text{---} \end{array} \left[\begin{array}{cccc} i \in \mathcal{I}_{\text{bsp}} \rightarrow & & & \\ * & * & * & \\ * & * & * & \\ & * & * & * \\ & & & \ddots \\ \text{---} & \text{---} & \text{---} & \text{---} \\ & & * & * & * \\ \text{---} & \text{---} & \text{---} & \text{---} & \text{---} \\ & & \underbrace{\hspace{2cm}}_{i \in \mathcal{I}_{\text{loc}}(\hat{k})} & & \end{array} \right]$$

Remark 2 (Choice of the index sets). Let $\text{supp } \tilde{\psi}_{\hat{k}} = (\zeta_{k_l}, \zeta_{k_r})$, consider the central element $\hat{e} = e_{\lfloor (k_l + k_r) / 2 \rfloor}$. Then let $\mathcal{I}_{\text{loc}}(\hat{k})$ contain the $p + 1$ indices of the B-splines that are supported on the element \hat{e} :

$$\mathcal{I}_{\text{loc}}(\hat{k}) = \left\{ i \in \mathcal{I}_{\text{bsp}}, \hat{e} \subset \text{supp } \hat{B}_i^p \right\}.$$

The biorthogonal basis with local support and optimal approximation order p is then defined as

$$(7) \quad \hat{\psi}_i = \tilde{\psi}_i + \sum_{k \in \mathcal{J}_{\text{extra}}} z_{ki} \tilde{\psi}_k, \quad \text{for } i \in \mathcal{I}_{\text{bsp}}.$$

The support of $\hat{\psi}_i$ is determined by the choice of the index sets. Since $z_{ki} \neq 0$ yields $\text{supp } \tilde{\psi}_k \subset \text{supp } \hat{\psi}_i$, we can estimate the support of $\hat{\psi}_i$ by

$$\text{supp } \hat{\psi}_i \subset \text{supp } \hat{B}_i^p \cup \bigcup_{k \in \mathcal{I}_{\text{loc}}(i)} \text{supp } \tilde{\psi}_k.$$

By construction, the support of $\tilde{\psi}_j$ overlaps partially with the support of \hat{B}_i^p . Since it contains at most $p + 1$ elements, the support for the presented construction contains at most $2p + 1$ elements.

The following Theorem 1 concludes this section by proving the optimality of the constructed biorthogonal basis.

Theorem 1. Assume that for all $\hat{k} \in \mathcal{J}_{\text{extra}}$, the equation system (6) has full rank. Then the basis $(\hat{\psi}_i)_{i \in \mathcal{I}_{\text{bsp}}}$ defined by (7) is an optimal biorthogonal basis, i.e., it fulfills biorthogonality

$$\left(\hat{B}_i^p, \hat{\psi}_j \right)_{\hat{\rho}} = \delta_{ij},$$

for $i, j \in \mathcal{I}_{\text{bsp}}$ and optimal convergence on $M_h = \text{span}_i \widehat{\psi}_i$, i.e., for any $\lambda \in H^{p+1}(\Gamma)$

$$\inf_{\mu_h \in M_h} \|\mu_h - \lambda\|_{L^2(\Gamma)} \leq ch^{p+1} \|\lambda\|_{H^{p+1}(\Gamma)}.$$

Proof. The proof follows the ideas of the finite element case, see [29]. By construction of $(\widetilde{\psi}_i)_{i=1, \dots, N}$, for any choice of $(z_{ki})_{k,i}$,

$$\widetilde{\psi}_i + \sum_{k \in \mathcal{J}_{\text{extra}}} z_{ki} \widetilde{\psi}_k, \quad \text{for } i \in \mathcal{I}_{\text{bsp}},$$

is a biorthogonal basis to $(\widehat{B}_i^p)_{i \in \mathcal{I}_{\text{bsp}}}$.

Now, let us show that the choice of z_{ki} for $k \in \mathcal{J}_{\text{extra}}$ and $i \in \mathcal{I}_{\text{bsp}}$ guarantees polynomial reconstruction. Therefore, we show that the quasi-interpolation

$$\mathcal{Q}f = \sum_{i \in \mathcal{I}_{\text{bsp}}} (f, \widehat{B}_i^p)_{\widehat{\rho}} \widehat{\psi}_i$$

is invariant for polynomials \mathbb{P}_p , which is equivalent to

$$(p_l, \varphi_j)_{\widehat{\rho}} = \sum_{i \in \mathcal{I}_{\text{bsp}}} (p_l, \widehat{B}_i^p)_{\widehat{\rho}} (\widehat{\psi}_i, \varphi_j)_{\widehat{\rho}}, \quad \text{for any } j = 1, \dots, N, \quad l = 1, \dots, p+1.$$

For $j \in \mathcal{I}_{\text{bsp}}$ it holds that $\varphi_j = \widehat{B}_j^p$, and we can directly use the biorthogonality of $\widehat{\psi}_i$ and φ_j :

$$\sum_{i \in \mathcal{I}_{\text{bsp}}} (p_l, \widehat{B}_i^p)_{\widehat{\rho}} (\widehat{\psi}_i, \varphi_j)_{\widehat{\rho}} = \sum_{i \in \mathcal{I}_{\text{bsp}}} (p_l, \widehat{B}_i^p)_{\widehat{\rho}} \delta_{ij} = (p_l, \varphi_j)_{\widehat{\rho}}.$$

For $j \in \mathcal{J}_{\text{extra}}$, biorthogonality cannot be directly used, but the considered equation system (6) yields, since $\mathcal{I}_{\text{bsp}} \cap \mathcal{J}_{\text{extra}} = \emptyset$ and $z_{ji} = 0$ for $i \notin \mathcal{I}_{\text{loc}}(j)$:

$$\begin{aligned} \sum_{i \in \mathcal{I}_{\text{bsp}}} (p_l, \widehat{B}_i^p)_{\widehat{\rho}} (\widehat{\psi}_i, \varphi_j)_{\widehat{\rho}} &= \sum_{i \in \mathcal{I}_{\text{bsp}}} (p_l, \widehat{B}_i^p)_{\widehat{\rho}} \left(\widetilde{\psi}_i + \sum_{k \in \mathcal{J}_{\text{extra}}} z_{ki} \widetilde{\psi}_k, \varphi_j \right)_{\widehat{\rho}} \\ &= \sum_{i \in \mathcal{I}_{\text{bsp}}} (p_l, \widehat{B}_i^p)_{\widehat{\rho}} z_{ji} = \sum_{i \in \mathcal{I}_{\text{loc}}(j)} (p_l, \widehat{B}_i^p)_{\widehat{\rho}} z_{ji} = (p_l, \varphi_j)_{\widehat{\rho}}. \end{aligned}$$

□

At the end of this construction, the biorthogonal basis functions can be scaled as desired. A common scaling, e.g. [28], is

$$\int_{\Gamma} N_i \psi_j \, d\mathbf{\Gamma} = \delta_{ij} \int_{\Gamma} N_i \, d\mathbf{\Gamma}$$

The newly constructed biorthogonal basis functions are shown in Figure 3, where they are compared to the naive biorthogonal basis functions from [28] and the primal basis functions.

3.2. Multilateral construction by tensorization. We set $\rho \circ \mathbf{F} = \widehat{\mathcal{W}} / \det \nabla_{\widehat{\mathbf{F}}} \mathbf{F}$, such that $\widehat{\rho} = 1$. Since the interface in the parametric space is a direct tensor-product of one-dimensional spline spaces, we can construct the biorthogonal basis as a tensor product.

As a geometric interpretation, $\widehat{\rho} = 1$ means that the coupling condition is posed in the parametric space, instead of the geometric space, see Figure 4. This is valid, since the surface measure on the parametric space and the geometric space are mathematically equivalent. The advantage is that we can directly profit from the

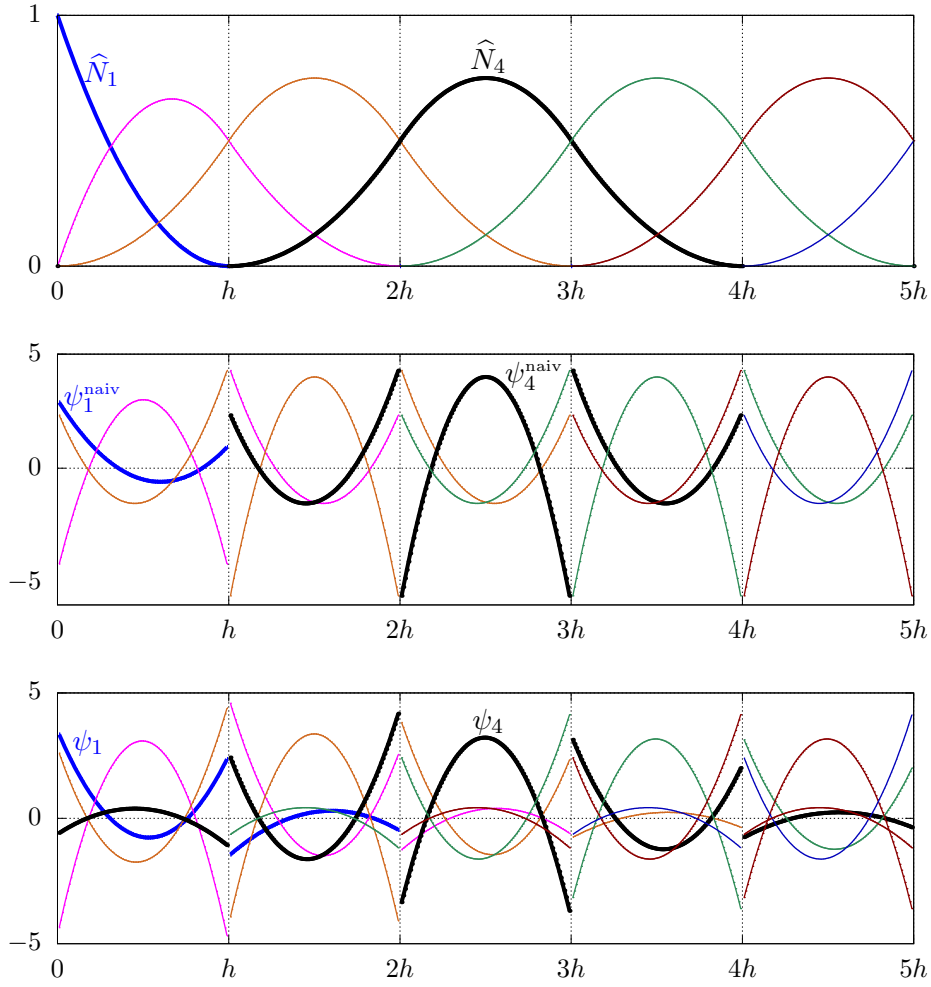


FIGURE 3. Primal (top), naive dual (middle) and optimal dual (bottom) basis functions shown on the first five elements of a quadratic spline patch with the first and fourth basis function being highlighted in bold.

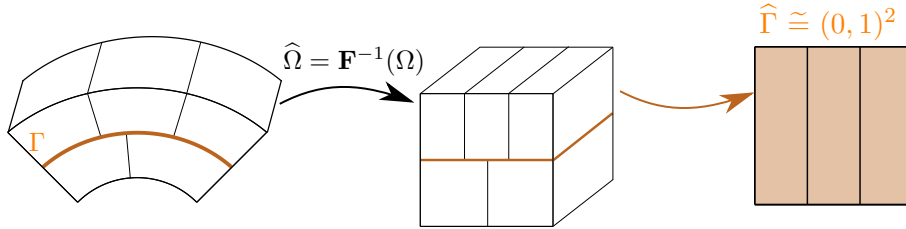


FIGURE 4. Illustration of the mapping to the parametric space.

tensor product construction on $\Gamma = (0, 1)^2 \times \{0\}$. With the tensor product B-spline basis

$$\widehat{B}_{(i,j)}(\zeta_1, \zeta_2) = \widehat{B}_i^p(\zeta_1) \widehat{B}_j^p(\zeta_2),$$

the tensor product of a univariate biorthogonal basis ψ_i , viz.

$$\widehat{\psi}_{(i,j)}(\zeta_1, \zeta_2) = \widehat{\psi}_i^p(\zeta_1) \widehat{\psi}_j^p(\zeta_2),$$

forms a multivariate biorthogonal basis:

$$\begin{aligned} & \int_{\Gamma} \widehat{B}_{(i,j)}(\zeta_1, \zeta_2) \widehat{\psi}_{(k,l)}(\zeta_1, \zeta_2) \, d(\zeta_1, \zeta_2) \\ (8) \quad & = \int_0^1 \widehat{B}_i(\zeta_1) \widehat{\psi}_k(\zeta_1) \, d\zeta_1 \int_0^1 \widehat{B}_j(\zeta_2) \widehat{\psi}_l(\zeta_2) \, d\zeta_2 = \delta_{ik} \delta_{jl}. \end{aligned}$$

Of course, the polynomial reproduction order is retained with the tensor product construction.

For different choices of ρ , the integrals in (8) are weighted with $\widehat{\rho} \neq 1$. Then, in general, the integral cannot be separated into two independent integrals, hence the constructed basis is not biorthogonal.

With two-dimensional interfaces, ‘crosspoints’ are entire boundary faces, due to our regularity assumptions of Section 2.2. By a simple crosspoint modification for the one-dimensional bases that are used in the tensor-product construction, we conveniently get a crosspoint modification also of the two-dimensional basis. Note that, when the ‘crosspoints’ are only a subset of the boundary faces, still a crosspoint modification can safely be performed on the entire boundary face.

4. NUMERICAL RESULTS

In the following, we test our newly constructed biorthogonal basis on three numerical examples and compare it with the naive biorthogonal basis from [28] as well as standard Lagrange multipliers. Where an exact solution is available, the L^2 -error is considered, in the other cases convergence is studied by observing the internal energy as well as point evaluations. All numerical computations are performed with the in-house research code BACI [38].

4.1. Plate with a hole. As the first example, we consider the well-known benchmark of an infinite plate with a hole, e.g. [39, §58]. Due to symmetry, only a quarter of the plate is considered, and the infinite geometry is cut with the exact traction being applied as a boundary condition. The exact setting is illustrated in Figure 5.

We consider the equations of linear elasticity, where the Cauchy stress $\boldsymbol{\sigma}(\mathbf{u})$ depends linearly on the strain $\boldsymbol{\varepsilon}(\mathbf{u}) = 1/2 (\nabla \mathbf{u} + (\nabla \mathbf{u})^\top)$ via Hooke’s law as $\boldsymbol{\sigma}(\mathbf{u}) = 2\mu \boldsymbol{\varepsilon}(\mathbf{u}) + \lambda \operatorname{tr} \boldsymbol{\varepsilon}(\mathbf{u}) \operatorname{Id}$, with the trace operator $\operatorname{tr} \boldsymbol{\varepsilon} = \sum_i \varepsilon_{ii}$ and the Lamé parameters λ, μ . The Lamé parameters can be computed by

$$\lambda = \frac{\nu E}{(1 + \nu)(1 - 2\nu)}, \quad \mu = \frac{E}{2(1 + \nu)}.$$

We measure convergence in the energy norm

$$\|\mathbf{u} - \mathbf{u}_h\|_E^2 = \sum_k \int_{\Omega_k} \boldsymbol{\sigma}(\mathbf{u} - \mathbf{u}_h) : \boldsymbol{\varepsilon}(\mathbf{u} - \mathbf{u}_h) \, d\mathbf{X},$$

where the optimal convergence order is $\mathcal{O}(h^p)$, see [19, Theorem 6].

Different geometry parametrizations are considered, as shown in Figure 6. The first case (Figure 6a) is a two-patch setting with a straight interface, where the parametrization of the interface is the same on both subdomains. In the second case (Figure 6b) the same subdomains are considered, but with a different parametrization, such that the parametrizations along the interface do no longer match. We note, that this is a situation, where the construction of [31] is not exact, but requires additional steps of refinement. In the third case (Figure 6c), the subdomains are coupled across a curved interface.

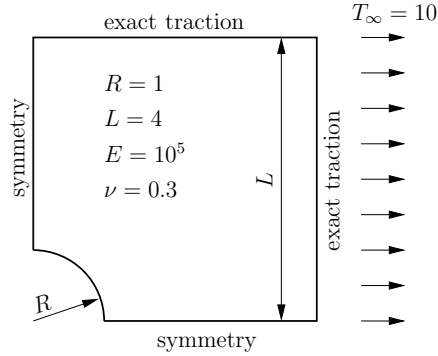


FIGURE 5. Plate with a hole: Geometry, boundary conditions and material parameters.

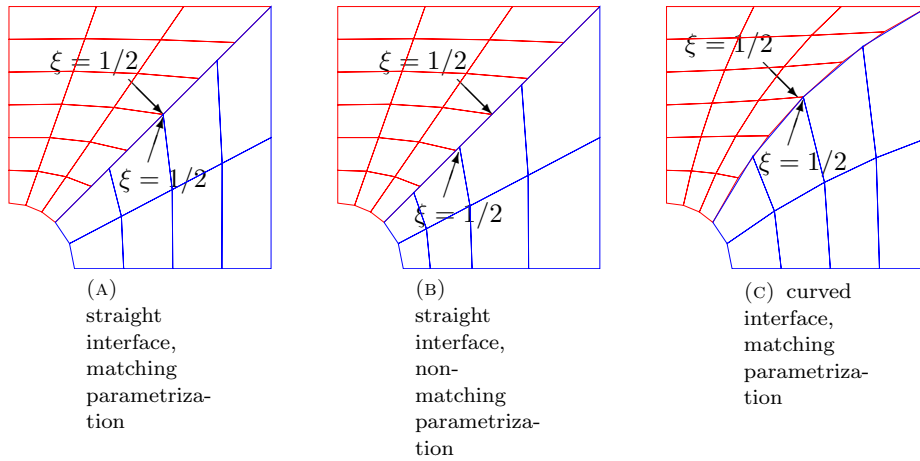


FIGURE 6. Different geometric setups of the plate with hole, shown for the mesh ratio 2 : 3.

For all three setups, convergence for quadratic splines and different Lagrange multiplier bases is presented in Figure 7. We observe an optimal order convergence for the newly constructed biorthogonal basis functions ('optimal'), with similar error values as with a standard Lagrange multiplier ('std'). In comparison, the naive, element-wise biorthogonal basis functions ('ele dual') as considered in [28] show suboptimal convergence, especially when the slave mesh is coarser than the master mesh.

The same comparisons for cubic splines are shown in Figure 8. Again, we see an optimal order convergence of the optimal biorthogonal basis functions as expected theoretically, while the suboptimality of the naive biorthogonal basis functions from [28] becomes even more apparent. However, when the slave mesh is coarser than the master mesh, the values of the error are larger than for the standard Lagrange multiplier case. Since the gap gets smaller with further refinements, this seems to be a pre-asymptotical effect. We note that for a fine slave mesh, no significant suboptimality can be observed in the pre-asymptotics.

In summary, we have observed optimal convergence rates in all cases for the newly constructed biorthogonal basis functions, while suboptimal rates were seen for the naive biorthogonal basis from [28]. When the finer side is chosen as the

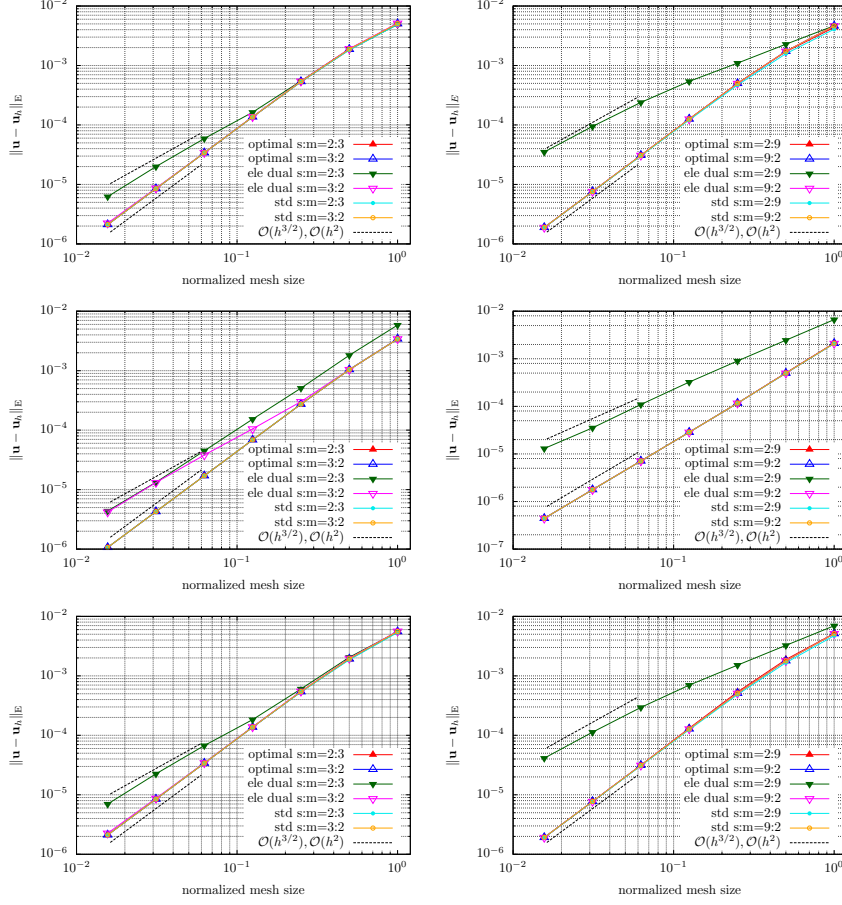


FIGURE 7. Convergence of the energy error for $p = 2$. Comparison of the new biorthogonal basis ('optimal'), standard dual basis ('ele dual') and standard Lagrange multipliers ('std'). Left: mesh ratio 2 : 3. Right: mesh ratio 2 : 9. From top to bottom the three mesh cases (a) to (c) from Figure 6 are considered.

slave side, the error values were the same as for standard Lagrange multipliers. Only when the slave side is coarser, a suboptimal preasymptotic evolves. Hence, for the optimal biorthogonal basis, it is especially important to choose the finer side of the interface as the slave side, whenever this is possible.

4.2. Bimaterial annulus. In the second example, we consider a two-dimensional bimaterial setting. The bimaterial annulus shown in Figure 9 consists of a soft material ($E_1 = 1e3$, $\nu_1 = 0.3$) with a thin hard inclusion ($E_2 = 1e5$, $\nu_2 = 0.3$) with an elliptic interface. The considered geometry parameters are:

$$\begin{aligned} r_i &= 0.75, & r_o &= 1, \\ a_1 &= 0.55(r_i + r_o - 1) = 0,95975, & b_1 &= 0.5(r_i + r_o - 1)/1.1 \approx 0,7932, \\ a_2 &= 0.55(r_i + r_o + 1) = 0,96525, & b_2 &= 0.5(r_i + r_o + 1)/1.1 \approx 0,7977. \end{aligned}$$

Inside the annulus, a constant unit-pressure is applied, and the outer boundary is a homogeneous Neumann boundary. The rigid body modes are removed by restricting the corresponding deformations.

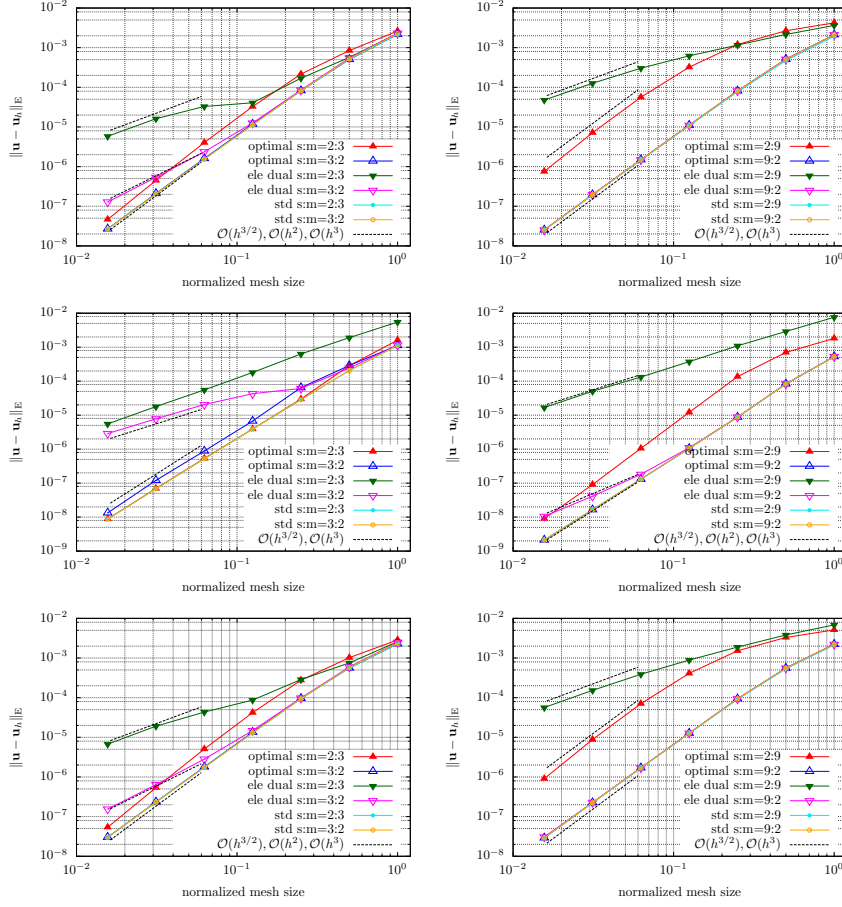


FIGURE 8. Convergence of the energy error for $p = 3$. Comparison of the new biorthogonal basis ('optimal'), standard dual basis ('ele dual') and standard Lagrange multipliers ('std'). Left: mesh ratio 2 : 3. Right: mesh ratio 2 : 9. From top to bottom the three mesh cases (a) to (c) from Figure 6 are considered.

The different stiffnesses and the thin geometry of the inclusion demand for anisotropic elements and different mesh-sizes in the different subdomains. The interior subdomain consists of 20 elements in the angular direction and three elements in the radial direction, the thin inclusion consists of 68 elements in the angular direction and one element in the radial direction, and the outer subdomain consists of 24 element in the angular direction and two elements in the radial direction.

In Figure 10, convergence of the energy $E = \int_{\Omega} \boldsymbol{\sigma}(\mathbf{u}) : \boldsymbol{\varepsilon}(\mathbf{u}) \, d\mathbf{X}$ is presented. Lacking the exact solution, we use a reference value on a refined mesh $E_{\text{ref}} \approx 3.59e-3$. Again, we clearly see the suboptimality of the naive biorthogonal basis functions from [28], which exhibit a convergence of the order $h^{3/2}$. In the second order case, the optimal biorthogonal basis shows the same approximation quality as the standard Lagrange multiplier, independent of the choice of the slave side. In the third order case, a suboptimal pre-asymptotic can again be observed for the case of a coarse slave mesh. Still, the error in the energy is smaller than for the naive biorthogonal basis. When the fine side is chosen as the slave space, again no

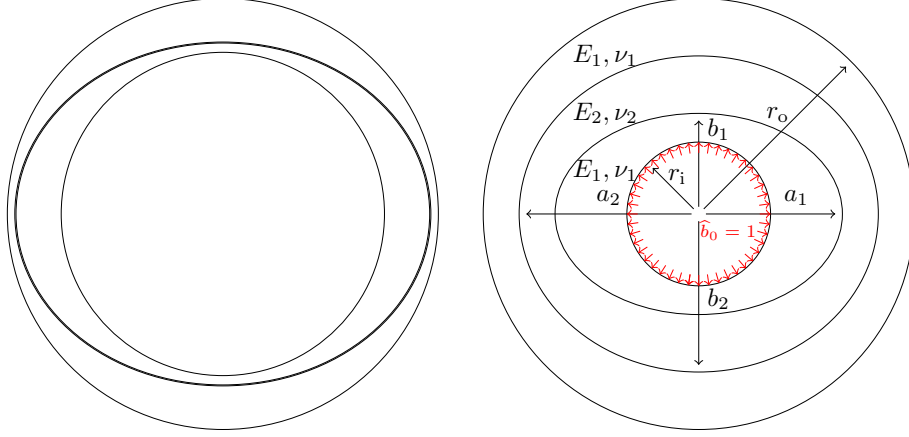


FIGURE 9. Geometry and problem setting. Left: Exact geometry. Right: Schematic plot with applied boundary traction.

difference in the approximation quality is seen between the optimal dual basis and the standard Lagrange multiplier.

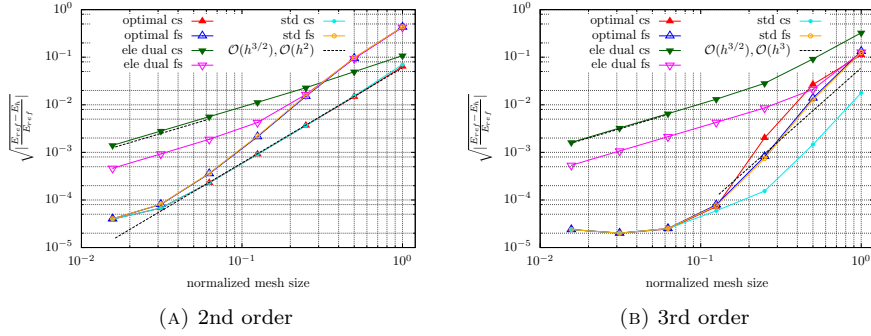


FIGURE 10. Convergence of the energy error for $p = 2$ and $p = 3$. In the fine slave ('fs') case, the thin inclusion layer with a finer (interface-) mesh is chosen as slave side (on both interfaces). In the coarse slave ('cs') case, the thin inclusion layer with a finer (interface-) mesh is chosen as master side (on both interfaces).

These results are of particular importance when comparing to [40, 41], where strong oscillations could be observed for curved interfaces for the finite element case. The reason why this is not observed here for isogeometric methods might be the exact representation of the curved interface.

4.3. Pressurized hollow sphere. The final example extends the previous setup to the three-dimensional case. We consider a pressurized hollow sphere with two 45° holes as shown in Figure 11. Again, there is a thin inclusion of a stiff material with an elliptical cross-section. More precisely, the equatorial plane resembles the two-dimensional geometry from Section 4.2. We choose the same material parameters as before, but consider a non-linear Neo-Hooke material:

$$\Psi(\mathbf{C}) = c(\text{tr}\mathbf{C} - 3) + \frac{c}{\beta}((\det \mathbf{C})^{-\beta} - 1),$$

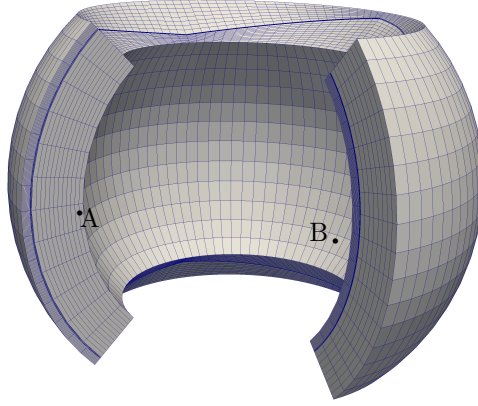


FIGURE 11. Bimaterial geometry with the front quarter removed for visualization.

with $c = E/(1 + 4\nu)$ and $\beta = \nu/(1 - 2\nu)$.

The final deformation for quadratic NURBS on 68 624 elements for the whole domain, with 104 016 control points is shown in Figure 14, which includes the circumferential Cauchy stress. As expected, the thin stiff inclusion carries most of the pressure. The biorthogonal basis guarantees an accurate and smooth transmission of the forces, and no oscillations across the interface can be seen at all.

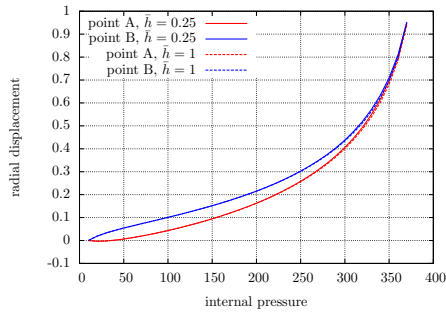


FIGURE 12. Radial displacement in relation to the internal pressure.

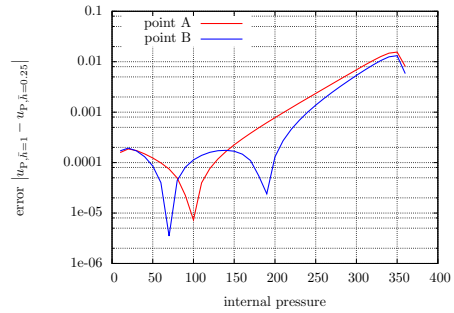


FIGURE 13. Estimated error of the displacements by comparison of $\bar{h} = 1$ to $\bar{h} = 0.25$.

We observe the radial displacements at two points A and B as shown in Figure 11 during the increase of the internal pressure, see Figure 12. The discretization error is estimated qualitatively by comparing to the values obtained on a coarser mesh, see Figure 13. We see a good agreement, since the computed displacements differ by a value of less than 0.02. For pressure values lower than 150, the difference is even less than $2e-4$.

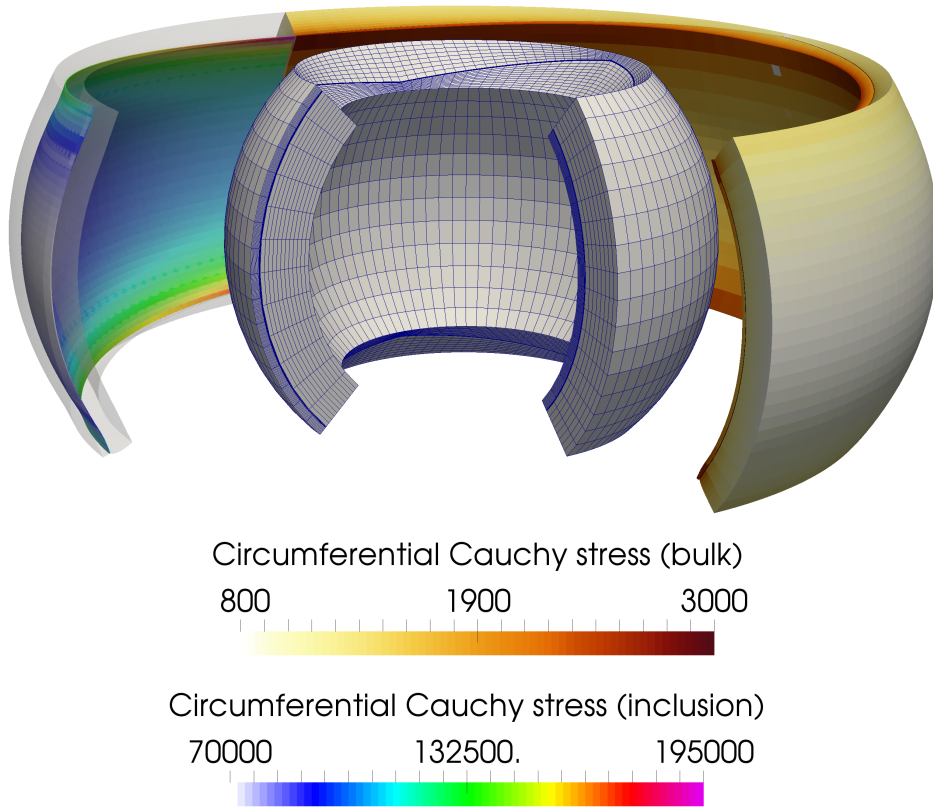


FIGURE 14. Deformed geometry with the circumferential Cauchy stress indicated.

5. CONCLUSIONS

We have investigated isogeometric methods with a newly constructed biorthogonal basis that yields optimal convergence rates. Thanks to the local support of the dual basis, the resulting equation system is sparse and elliptic. The new biorthogonal basis is proposed with a univariate construction, that is then adapted for two-dimensional interfaces by a tensor product. To preserve biorthogonality in the tensor product, we have to consider equivalent, weighted integrals. A crosspoint modification is inherently included in the one-dimensional construction.

The numerical results include finite deformations in 3D and confirm the optimal convergence. They also show that, whenever possible, the slave side should be chosen as the finer mesh, since a suboptimal pre-asymptotic is observed for coarse slave spaces. Finally, a three-dimensional bimaterial example with finite deformations qualitatively confirms the suitability and efficiency of the method for large-scale engineering applications.

REFERENCES

- [1] J. A. Cottrell, A. Reali, Y. Bazilevs, T. J. R. Hughes, Isogeometric analysis of structural vibrations, *Comput. Methods Appl. Mech. Eng.* 195 (41–43) (2006) 5257 – 5296.
- [2] J. A. Cottrell, T. J. R. Hughes, Y. Bazilevs, *Isogeometric Analysis. Towards Integration of CAD and FEA*, Wiley, Chichester, 2009.
- [3] L. Beirão Da Veiga, A. Buffa, G. Sangalli, R. Vázquez, Mathematical analysis of variational isogeometric methods, *Acta Numer.* 23 (2014) 157–287.

- [4] V. P. Nguyen, C. Anitescu, S. P. A. Bordas, T. Rabczuk, Isogeometric analysis: An overview and computer implementation aspects, *Math. Comp. Simul.* 117 (2015) 89 – 116.
- [5] K. Höllig, *Finite Element Methods with B-Splines*, *Frontiers in Applied Mathematics*, SIAM, 2003.
- [6] V. P. Nguyen, P. Kerfriden, M. Brino, S. P. A. Bordas, E. Bonisoli, Nitsche’s method for two and three dimensional NURBS patch coupling, *Comput. Mech.* 53 (6) (2014) 1163–1182.
- [7] A. Apostolatos, R. Schmidt, R. Wüchner, K.-U. Bletzinger, A Nitsche-type formulation and comparison of the most common domain decomposition methods in isogeometric analysis, *Int. J. Numer. Methods Eng.* 97 (2014) 473–504.
- [8] C. Hofer, U. Langer, I. Touloupoulos, Discontinuous Galerkin isogeometric analysis on non-matching segmentation: Error estimates and efficient solvers, *Tech. Rep. 2016-23*, RICAM, Linz, Austria (2016).
- [9] W. Dornisch, G. Vitucci, S. Klinkel, The weak substitution method – an application of the mortar method for patch coupling in NURBS-based isogeometric analysis, *Int. J. Numer. Methods Eng.* 103 (3) (2015) 205–234.
- [10] C. Hesch, P. Betsch, Isogeometric analysis and domain decomposition methods, *Comput. Methods Appl. Mech. Eng.* 213–216 (2012) 104–112.
- [11] L. Coox, F. Greco, O. Atak, D. Vandepitte, W. Desmet, A robust patch coupling method for NURBS-based isogeometric analysis of non-conforming multipatch surfaces, *Comput. Methods Appl. Mech. Eng.* 316 (2017) 235–260.
- [12] T. Horger, A. Reali, B. Wohlmuth, L. Wunderlich, A hybrid isogeometric approach on multipatches with applications to Kirchhoff plates and eigenvalue problems, in preparation.
- [13] B. Marussig, T. J. R. Hughes, A review of trimming in isogeometric analysis: Challenges, data exchange and simulation aspects, *Arch. Comput. Methods Eng.* (2017) 1–69.
- [14] L. De Lorenzis, P. Wriggers, T. J. R. Hughes, Isogeometric contact: a review, *GAMM-Mitt.* 37 (1) (2014) 85–123.
- [15] P. Antolin, A. Buffa, M. Fabre, A priori error for unilateral contact problems with Lagrange multiplier and isogeometric analysis, <https://arxiv.org/abs/1701.03150>.
- [16] F. Ben Belgacem, The mortar finite element method with Lagrange multipliers, *Numer. Math.* 84 (1999) 173–197.
- [17] C. Bernardi, Y. Maday, A. T. Patera, A new nonconforming approach to domain decomposition: the mortar element method, in: H. B. et.al. (Ed.), *Nonlinear partial differential equations and their applications.*, Vol. XI, Collège de France, 1994, pp. 13–51.
- [18] B. Wohlmuth, *Discretization Techniques and Iterative Solvers Based on Domain Decomposition*, Vol. 17 of *Lectures Notes in Computational Science and Engineering*, Springer, Heidelberg, 2001.
- [19] E. Brivadis, A. Buffa, B. Wohlmuth, L. Wunderlich, Isogeometric mortar methods, *Comput. Methods Appl. Mech. Eng.* 284 (2015) 292–319.
- [20] B. Wohlmuth, A mortar finite element method using dual spaces for the Lagrange multiplier, *SIAM J. Numer. Anal.* 38 (2000) 989–1012.
- [21] A. Popp, M. W. Gee, W. A. Wall, A finite deformation mortar contact formulation using a primal-dual active set strategy, *Int. J. Numer. Methods Eng.* 79 (11) (2009) 1354–1391.
- [22] A. Popp, M. Gitterle, M. W. Gee, W. A. Wall, A dual mortar approach for 3D finite deformation contact with consistent linearization, *Int. J. Numer. Methods Eng.* 83 (11) (2010) 1428–1465.
- [23] A. Popp, A. Seitz, M. W. Gee, W. A. Wall, Improved robustness and consistency of 3D contact algorithms based on a dual mortar approach, *Comput. Methods Appl. Mech. Eng.* 264 (2013) 67–80.
- [24] A. Popp, W. A. Wall, Dual mortar methods for computational contact mechanics - overview and recent developments, *GAMM-Mitt.* 37 (1) (2014) 66–84.
- [25] B. Lamichhane, B. Wohlmuth, Biorthogonal bases with local support and approximation properties, *Math. Comp.* 76 (257) (2007) 233–249.
- [26] B. Wohlmuth, A. Popp, M. W. Gee, W. A. Wall, An abstract framework for a priori estimates for contact problems in 3D with quadratic finite elements, *Comput. Mech.* 49 (2012) 735–747.
- [27] A. Popp, B. Wohlmuth, M. W. Gee, W. A. Wall, Dual quadratic mortar finite element methods for 3D finite deformation contact, *SIAM J. Sci. Comp.* (2012) B421–B446.
- [28] A. Seitz, P. Farah, J. Kremheller, B. Wohlmuth, W. A. Wall, A. Popp, Isogeometric dual mortar methods for computational contact mechanics, *Comput. Methods Appl. Mech. Eng.* 301 (2016) 259–280.
- [29] P. Oswald, B. Wohlmuth, On polynomial reproduction of dual FE bases, in: N. Debit, M. Garbey, R. Hoppe, D. Keyes, Y. Kuznetsov, J. Périaux (Eds.), *Domain Decomposition Methods in Science and Engineering*, CIMNE, 2002, pp. 85–96, 13th International Conference on Domain Decomposition Methods, Lyon, France.

- [30] W. Dornisch, J. Stöckler, R. Müller, Dual and approximate dual basis functions for B-splines and NURBS Comparison and application for an efficient coupling of patches with the isogeometric mortar method, *Comput. Methods Appl. Mech. Eng.* 316 (2017) 449 – 496.
- [31] Z. Zou, M. Scott, M. Borden, D. Thomas, W. Dornisch, E. Brivadis, Isogeometric Bézier dual mortaring: Refineable higher-order spline dual bases and weakly continuous geometry, *Comput. Methods Appl. Mech. Eng.* 333 (2018) 497 – 534.
- [32] E. Brivadis, A. Buffa, B. Wohlmuth, L. Wunderlich, The influence of quadrature errors on isogeometric mortar methods, in: B. Jüttler, B. Simeon (Eds.), *Isogeometric Analysis and Applications 2014*, Springer International Publishing, Cham, 2015, pp. 33–50.
- [33] Y. Maday, F. Rapetti, B. Wohlmuth, The influence of quadrature formulas in 2D and 3D mortar element methods., in: *Recent developments in domain decomposition methods. Some papers of the workshop on domain decomposition*, ETH Zürich, Switzerland, June 7–8. 2001, Springer, 2002, pp. 203–221.
- [34] L. Cazabeau, C. Lacour, Y. Maday, Numerical quadrature and mortar methods, in: *Computational Science for the 21st Century*, John Wiley and Sons, 1997, pp. 119–128.
- [35] P. Farah, A. Popp, W. A. Wall, Segment-based vs. element-based integration for mortar methods in computational contact mechanics, *Comput. Mech.* 55 (1) (2015) 209–228.
- [36] D. Boffi, F. Brezzi, M. Fortin, *Mixed Finite Element Methods and Applications*, Springer, Berlin, 2013.
- [37] M. Benzi, G. H. Golub, J. Liesen, Numerical solution of saddle point problems, *Acta Numer.* 14 (2005) 1–137.
- [38] W. A. Wall, M. Kronbichler, BACI: A multiphysics simulation environment, Tech. rep., Technische Universität München (2018).
- [39] N. I. Muskhelishvili, *Some Basic Problems of the Mathematical Theory of Elasticity*, Springer, 1977, translated from the Russian.
- [40] B. Flemisch, M. Puso, B. Wohlmuth, A new dual mortar method for curved interfaces: 2D elasticity, *Internat. J. Numer. Methods Eng.* 63 (2005) 813–832.
- [41] B. Flemisch, B. Wohlmuth, Stable Lagrange multipliers for quadrilateral meshes of curved interfaces in 3D, *Comput. Methods Appl. Mech. Eng.* 196 (2007) 1589–1602.